



A Modified MPPT-SRF Configuration of a Single Stag Grid-Connected PV System Inverter Based on Voltage-Oriented Control

Dindu Venkata Koteswara Rao, O. Ranjit Kumar

PG Scholar (Power Electronics and Drives), Department of Electrical & Electronics Engineering, QIS Institute of Technology, Ongole, A.P, India.

Assistant Professor, Department of Electrical & Electronics Engineering, QIS Institute of Technology, Ongole, A.P, India.

ABSTRACT: A Modified MPPT-SRF Configuration of a Single Stag Grid-Connected PV System Inverter Based On Voltage-Oriented Control is shows better performance in conversion of PV output power into high-quality ac voltage. Hear the purpose of voltage-oriented control (VOC) is to solve fast varying irradiation problems. In VOC, a cascaded control structure with an outer dc link voltage control loop and an inner current control loop is used. The currents are controlled in a synchronous orthogonal d-q frame using a decoupled feedback control. The reference current of proportional–integral (PI) d-axis controller is replaced with FUZZY controller to improve the fastness of the triggering circuit of the VSI. With this we can achieve a unity power factor, the q-axis reference is set to zero and wave distortion are reduced which gives an improved efficiency. Simulations and experimental results demonstrate that the proposed method provides effective, fast, and perfect tracking. The results are examined by using MATLAB software.

I. INTRODUCTION

The voltage-power characteristic of a photovoltaic (PV) array is nonlinear and time varying because of the changes caused by the atmospheric conditions. The task of a maximum power point (MPP) tracking (MPPT) in a PV power system is to continuously tune the system so that it draws maximum power from the PV array. In recent years, the grid connected PV systems have become more popular because they do not need battery backups to ensure MPPT. The two typical configurations of a grid-connected PV system are single or two stages. In two stages, the first is used to boost the PV array voltage and track the maximum power; the second allows the conversion of this power into high-quality ac voltage.

The presence of several power stages undermines the overall efficiency, reliability, and compactness of the system besides increasing the cost. The single stage has numerous advantages, such as simple topology, high efficiency, etc. Nevertheless, the control strategy (FZZY Logic) has to be designed in order to extract the maximum available power and to properly transfer it from the PV array to the grid simultaneously. In this case, an important consideration in the controller design is needed.

In this paper, the main component of the single-stage grid connected PV system is the three-phase voltage source inverter (VSI). Typically, simple inductors L are used as a filter interfacing inverter and mains, as shown in Fig. 1. LCL filter provides advantages in costs and dynamics since smaller inductors can be used. However, in a grid-connected system, an LCL filter may cause resonance, which is a disaster for the system's stability. Hence, control systems involving LCL filters are inevitably more complicated. The voltage-oriented control (VOC) method used for VSI employs an outer dc link voltage control loop and an inner current control loop to achieve fast dynamic response. The performance of the power flow depends largely on the quality of the applied current control strategy. In this paper, the current control has been implemented in a rotating synchronous reference frame d, q because the controller can eliminate a steady-state error and has fast transient response by decoupling control.

International Journal of Advanced Research in Electrical, Electronics and Instrumentation Engineering

(An ISO 3297: 2007 Certified Organization)

Vol. 3, Issue 11, November 2014

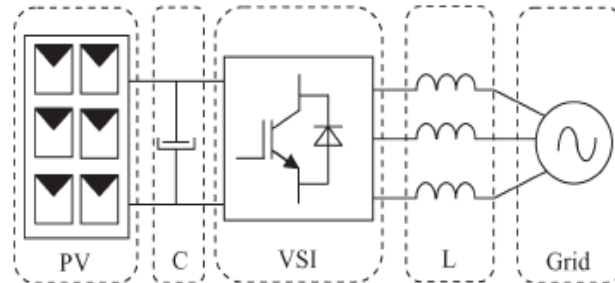


Fig. 1. Typical configuration of a single-stage grid-connected PV system.

Many algorithms have been developed for the MPPT of a PV array. Among the MPPT techniques, the perturbation and observation (P&O) method is the most popular because of the simplicity of its control structure. Yet, in the presence of rapidly changing atmospheric conditions, the P&O MPPT algorithm can be confused due to the fact that it is not able to distinguish the variations of the output power caused by the tracker perturbation from those caused by the irradiance variation. Recently, improved P&O MPPT algorithms for rapidly changing environmental conditions have been proposed by Sera *et al.* In this paper, in order to generate the correct MPP reference voltage under rapidly changing irradiation, a robust MPPT controller has been proposed. In this algorithm, the *d*-axis grid current component reflecting the power grid side and the signal error of a FUZZY Logic controller instead of PI controller outer voltage regulator is designed to reflect the change in power caused by the irradiation variation. Hence, with this information, the proposed algorithm can greatly reduce the power losses caused by the dynamic tracking errors under rapid weather changing conditions. The superiority of the newly proposed method is supported by simulation and experimental results.

II. SYSTEM DESCRIPTION AND MODELING

Fig. 1 shows the basic structure of a single-stage three-phase grid-connected PV system studied in this paper. This system consists of a PV array, an input filter capacitor *C*, a three-phase VSI, an output filter inductor *L*, and grid. The PV modules are connected in a series-parallel configuration to match the required dc voltage and power rating. The input capacitor supports the solar array voltage for the VSI. The three-phase pulse width-modulated inverter with a filter inductor converts a dc input voltage into an ac sinusoidal voltage by means of appropriate switch signals to make the output current in phase with the utility voltage and obtain a unity power factor.

A. Solar Cell and PV Array Model

A PV generator is a combination of solar cells, connections, protective parts, supports, etc. In the present modeling, the focus is only on cells. Solar cells consist of a p-n junction; various modeling's of solar cells have been proposed in the literature. Thus, the simplest equivalent circuit of a solar cell is a current source in parallel with a diode. The output of the current source is directly proportional to the light falling on the cell (photocurrent). During darkness, the solar cell is not an active device; it works as a diode, i.e., a p-n junction. It produces neither a current nor a voltage. Thus, the diode determines the *I-V* characteristics of the cell. For this paper, the electrical equivalent circuit of a solar cell is shown in Fig. 2 The output current *I* and the output voltage of a solar cell are given by

$$I = I_{ph} - I_{do} - \frac{V_{do}}{R_{sh}} = I_{ph} - I_0 \left(\exp\left(\frac{qV_{do}}{n.k.T}\right) - 1 \right) - \frac{V_{do}}{R_{sh}} \quad (1)$$

$$V = V_{do} - R_s I \quad (2)$$

Here, I_{ph} is the photocurrent, I_0 is the reverse saturation current, I_{do} is the average current through the diode, n is the diode factor, q is the electron charge ($q = 1.6 \times 10^{-19}$), k is

International Journal of Advanced Research in Electrical, Electronics and Instrumentation Engineering

(An ISO 3297: 2007 Certified Organization)

Vol. 3, Issue 11, November 2014

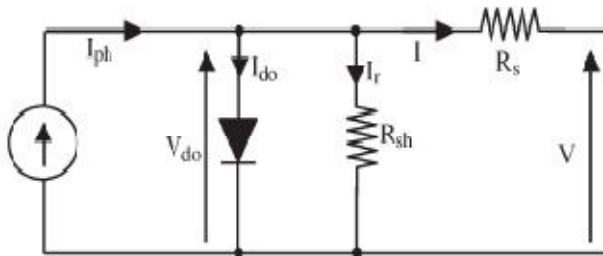


Fig. 2. Solar cell electrically equivalent circuit.

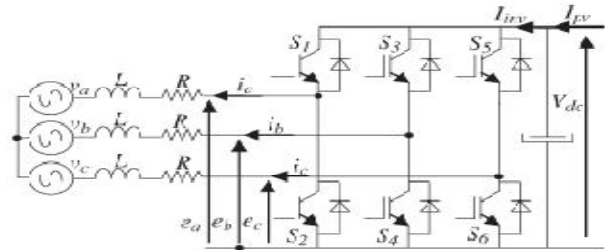


Fig. 3. Three-phase VSI.

the Boltzmann's constant ($k = 1.38 \times 10^{-23}$), and T is the solar array panel temperature. R_s is the intrinsic series resistance of the solar cell; this value is normally very small. R_{sh} is the equivalent shunt resistance of the solar array, and its value is very large. In general, the output current of a solar cell is expressed by

$$I = I_{ph} - I_0 \left(\exp \left(\frac{q}{n.k.T} (V + R_s I) \right) - 1 \right) - \left(\frac{V + R_s I}{R_{sh}} \right) \quad (3)$$

In (3), the resistances can be generally neglected, and thus, it can be simplified to

$$I = I_{ph} - I_0 \left(\exp \left(\frac{q}{n.k.T} V \right) - 1 \right) \quad (4)$$

If the circuit is opened, the output current $I = 0$, and the open-circuit voltage V_{oc} is expressed by

$$V_{oc} = \left(\frac{n.k.T}{q} \right) \ln \left(\frac{I_{ph}}{I_0} + 1 \right) \approx \left(\frac{n.k.T}{q} \right) \ln \left(\frac{I_{ph}}{I_0} \right) \quad (5)$$

If the circuit is shorted, the output voltage $V = 0$, the average current through the diode is generally neglected, and the short circuit current I_{sc} is expressed by using

$$I_{sc} = I = \frac{I_{ph}}{\left(1 + \frac{R_s}{R_{sh}} \right)} \quad (6)$$

Finally, the output power P is expressed by

$$P = VI = \left(I_{ph} - I_{do} - \frac{V_{do}}{R_{sh}} \right) V \quad (7)$$

III. VSI MODEL

The VSI connected to the grid through an L filter is shown in Fig. 3. In this section, a dynamic analytical model of the VSI is developed in its original three-phase abc frame. Then, this model is transformed into a synchronous reference frame. Before analyzing the three-phase VSI, some assumptions are proposed. The three-phase voltages are sinusoidal and symmetrical, and their representations are depicted in (8). The switches operate at constant frequency. The switching frequency is much higher than the line frequency. The inductors L are linear and balanced. Saturation is not a concern.

1) The whole conduction losses are represented by three symmetrical resistors R , as shown in Fig. 3. The absence of the zero sequence in the currents into a three wire system.

$$\begin{cases} V_a = V_m \cos(\omega t) \\ V_b = V_m \cos\left(\omega t - \frac{2}{3}\pi\right) \\ V_c = V_m \cos\left(\omega t + \frac{2}{3}\pi\right) \end{cases} \quad (8)$$

Based on the aforementioned assumptions, the model of the VSI in the stationary abc frame is established as

International Journal of Advanced Research in Electrical, Electronics and Instrumentation Engineering

(An ISO 3297: 2007 Certified Organization)

Vol. 3, Issue 11, November 2014

$$\left\{ \begin{array}{l} e_a = L \frac{di_a}{dt} + i_a R + v_a + v_n N \\ e_b = L \frac{di_b}{dt} + i_b R + v_b + v_n N \\ e_c = L \frac{di_c}{dt} + i_c R + v_c + v_n N \\ I_{pv} = C \frac{dV_{dc}}{dt} + I_{inv} \end{array} \right. \quad (9)$$

By doing the sum of the three equations in (9), one can obtain the relation

$$v_n N = \frac{1}{3}(e_a + e_b + e_c) \quad (10)$$

The switching function d^*k ($k = 1, 3, 5$) of the inverter is defined as in

$$d^*k = \begin{cases} 1, & \text{if } S_k \text{ is on and } S_{k+1} \text{ is off} \\ 0, & \text{if } S_k \text{ is off and } S_{k+1} \text{ is on} \end{cases} \quad (11)$$

Hence, one can write the complete model (12) of the VSI in the abc frame

$$\left\{ \begin{array}{l} L \frac{di_a}{dt} = -v_a - i_a R + \left(d^*_1 - \frac{d^*_1 + d^*_2 + d^*_3}{3} \right) V_{dc} \\ L \frac{di_b}{dt} = -v_b - i_b R + \left(d^*_2 - \frac{d^*_1 + d^*_2 + d^*_3}{3} \right) V_{dc} \\ L \frac{di_c}{dt} = -v_c - i_c R + \left(d^*_3 - \frac{d^*_1 + d^*_2 + d^*_3}{3} \right) V_{dc} \\ C \frac{dV_{dc}}{dt} = I_{pv} - (d^*_1 i_a + d^*_2 i_b + d^*_3 i_c) \end{array} \right. \quad (12)$$

For pulse width modulation (PWM) inputs, the aforementioned model can be separated into low- and high-frequency components using the Fourier analysis. The high-frequency model is concerned with the switching behavior of the inverter and is almost neglected. The low-frequency model, which has the same expression as (12), with the switching functions d^* being replaced by continuous duty ratios d_k ($k = 1, 3, 5$) $\in [0, 1]$, is much more considered

$$T_{dqo}^{abc} = \frac{2}{3} \begin{bmatrix} \cos(\omega t) & \cos\left(\omega t - \frac{2}{3}\pi\right) & \cos\left(\omega t + \frac{2}{3}\pi\right) \\ \sin(\omega t) & \sin\left(\omega t - \frac{2}{3}\pi\right) & \sin\left(\omega t + \frac{2}{3}\pi\right) \\ \frac{1}{2} & \frac{1}{2} & \frac{1}{2} \end{bmatrix} \quad (13)$$

It is noted that the model (12) is time varying and nonlinear. In order to facilitate the control, the model can be transformed into a synchronous orthogonal frame rotating at the angular frequency of the utility ω . With this time-varying transformation, given by (13), the positive sequence components at the fundamental frequency become constant. Finally, the whole dynamic model (14) in the dq frame is obtained from (12) and (13)

$$\begin{bmatrix} \frac{di_d}{dt} \\ \frac{di_q}{dt} \\ \frac{dV_{dc}}{dt} \end{bmatrix} = \begin{bmatrix} -\frac{R}{L} & \omega & \frac{d_d}{L} \\ \omega & -\frac{R}{L} & \frac{d_q}{L} \\ -\frac{d_d}{c} & -\frac{d_q}{c} & 0 \end{bmatrix} \begin{bmatrix} i_d \\ i_q \\ V_{dc} \end{bmatrix} + \begin{bmatrix} -\frac{1}{L} & 0 & 0 \\ 0 & -\frac{1}{L} & 0 \\ 0 & 0 & \frac{1}{c} \end{bmatrix} \begin{bmatrix} v_d \\ v_q \\ I_{pv} \end{bmatrix} \quad (14)$$

where

i_d, i_q d - and q -axis grid currents, respectively; v_d, v_q d - and q -axis grid voltages, respectively; d_d, d_q d - and q -axis duty ratios.

3.1 Current And Voltage Controllers

According to [19], VOC strategy guarantees fast transient response and high static performance via internal current control loops.

A. Current Control

It can be seen from (14) that there is cross-coupling between the d and q components. However, cross-coupling can affect the dynamic performance of the regulator. Therefore, it is very important to decouple the two axes for better performance. This effect can be accomplished with the feed forward decoupling control method. Assuming that

$$v_{rd} = -V_d + d_d V_{dc} + \omega L i_q$$

International Journal of Advanced Research in Electrical, Electronics and Instrumentation Engineering

(An ISO 3297: 2007 Certified Organization)

Vol. 3, Issue 11, November 2014

$$v_{rq} = -V_q + d_q V_{dc} - \omega L i_d \tag{15}$$

where ω is the angular frequency of the utility. Then, the system model is transformed to

$$\begin{cases} \frac{di_d}{dt} = -\frac{R}{L} i_d + \frac{1}{L} v_{rd} \\ \frac{di_q}{dt} = -\frac{R}{L} i_q + \frac{1}{L} v_{rq} \\ \frac{dV_{dc}}{dt} = \frac{I_{pv}}{C} - \frac{V_d + v_{rd}}{C V_{dc}} i_d - \frac{V_q + v_{rq}}{C V_{dc}} i_q \end{cases} \tag{16}$$

The cross-coupling variables are eliminated in the aforementioned model. Hence, the currents i_d and i_q can be controlled independently by acting upon inputs V_d and V_q , respectively. Furthermore, by using PI-type regulators, a fast dynamic response and zero steady-state errors can be achieved. The diagram of the current regulator is shown in Fig. 4. Since the switching frequency is much higher than the line frequency, the sampling and hold delay is neglected. the diagram, k_{ip} and k_{ii} are the proportional and integral parameters, respectively; i^* is the reference current signal, and I is the feedback current. The diagram is suitable for both i_d and

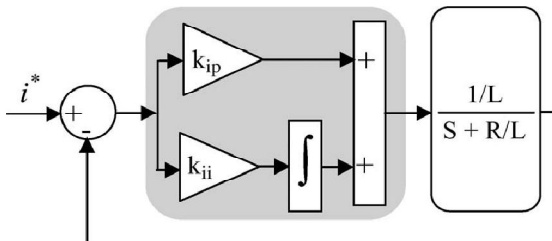


Fig. 4. Diagram of the current loop.

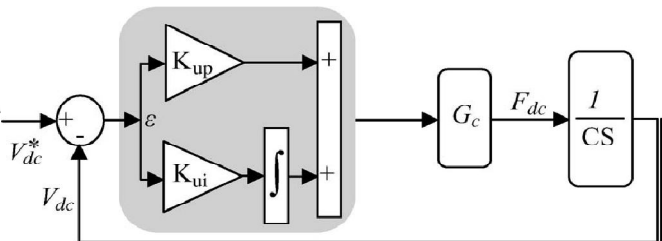


Fig. 5. Voltage loop diagram with constant irradiation.

i_q loops. From the diagram, the closed-loop transfer function of the d, q current loops is

$$\frac{i_q(s)}{i_q^*(s)} = \frac{i_d(s)}{i_d^*(s)} = \frac{k_{ip}}{L} \frac{s + \frac{k_{ii}}{k_{ip}}}{s^2 + \frac{(k_{ip} + R)}{L} s + \frac{k_{ii}}{L}} \tag{17}$$

The damping ratio $\zeta = (k_{ip} + R)/2L\sqrt{k_{ii}/L}$, and $\omega_n^2 = k_{ii}/L$. Thus, the parameters of the current regulator can be designed as follows:

$$k_{ip} = 2\zeta\omega_n L - R \tag{18}$$

$$k_{ii} = L\omega_n^2$$

B. Voltage Control

In the case of a unity power factor ($i_q = 0$) and with the previous assumption, the third equation in the model (14) is repeated as

$$C \frac{dv_{dc}}{dt} = I_{pv} - d_d i_d \tag{19}$$

At the beginning of a sequence, the atmospheric conditions are considered constant; hence, an equivalent input is defined as

$$F_d = I_{pv} - d_d i_d \tag{20}$$

In order to regulate the dc voltage at a fixed value, the error $\epsilon = V_{dc}^* - V_{dc}$ is passed through a PI-type compensator, as shown in Fig. 5.

In the diagram, the voltage loop is an outer loop, while the current loop is an inner loop. The internal loop has been designed to achieve short settling times in order to achieve a fast correction of the error. The outer loop can be designed to be slower. Thus, the inner and outer loops can be considered decoupled, and they can be linearized. Consequently, the current loop transfer function is approximately considered as $G_c = 1$.

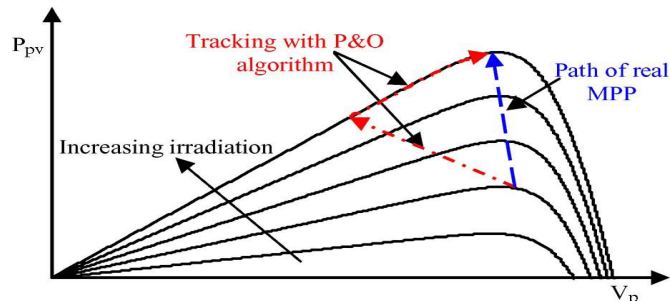


Fig. 6. Deviation from the MPP with the P&O algorithm under rapidly changing irradiance.

The closed-loop transfer function of dc voltage regulation, obtained from Fig. 5, has the following form:

$$\frac{V_{dc}(s)}{V_{dc}^*(s)} = \frac{k_{up} \frac{k_{ui} + s}{k_{up}}}{c s^2 + \frac{k_{up}}{c} s + \frac{k_{ui}}{c}} \quad (21)$$

In the same way as the design process of the current loop, the voltage regulator parameters can be given as follows:

$$\begin{aligned} k_{up} &= 2\zeta C \omega_{nu} \\ K_{ui} &= C \omega_{nu}^2 \end{aligned} \quad (22)$$

3.2 MPPT

The dc voltage controller is used to produce the reference current value for the *id* current controller. Its aim is to keep the voltage constant on the dc side in normal condition or during rapidly changing atmospheric conditions. The MPPT algorithm modulates the reference voltage V^*_{dc} according to the environmental conditions in order to keep the operating point of the PV panels close to the MPP. In the conventional P&O method, the MPP is obtained from the PV array power by multiplying the voltage and current of PV arrays and comparing it with the previously measured power. In the case of a sudden increase in irradiance, the P&O algorithm reacts as if the increase occurred as a result of the previous perturbation of the array operating voltage. The next perturbation, therefore, will be in the same direction as the previous one. Assuming that the system has been initially oscillating around the MPPT, the path of this behavior is drawn in Fig. 6. It can be seen that a continuous perturbation in one direction will lead to an operating point far away from the actual MPP. This process continues until the increase in irradiance slows down or ends.

The MPPT controller is applied to the reference of the outer loop control dc voltage photovoltaic (PV). Without PV array power measurement, the proposed MPPT identifies the correct direction of the MPP by processing the d-axis current reflecting the power grid side and the signal error of the FUZZY outer loop designed to only represent the change in power due to the changing atmospheric conditions. The robust tracking capability under rapidly increasing and decreasing irradiance is verified experimentally with a PV array emulator. To overcome the limitations of the P&O method, the proposed MPPT enables us to decouple the change in power caused by the simultaneous increment perturbation and irradiation variation. The irradiation variation is estimated by using the signal error of the PI controller of the dc voltage control. The PI regulator is designed to assure zero signal error if the atmospheric conditions are constant and a constant signal error in the opposite case. Hence, the signal error reflects only the change in power caused by the irradiation variation. After that, in order to calculate the total change in the PV array power, the *d*-axis grid current component is used. Finally, the change in power caused by the previous perturbation is obtained by a simple subtraction; therefore, the correct direction of the MPP can be identified.

A. PV Power Calculation

In the synchronous rotating frame *d, q*, the active and reactive powers of a three-phase grid-connected VSI are given by

$$\begin{cases} P = \frac{3}{2}(V_d i_d + V_q i_q) \\ Q = \frac{3}{2}(V_d i_q - V_q i_d) \end{cases} \quad (23)$$

If the three-phase grid voltage is ideally sinusoidal without any harmonics, then in the *d, q* frame, the grid voltage vector is given by

International Journal of Advanced Research in Electrical, Electronics and Instrumentation Engineering

(An ISO 3297: 2007 Certified Organization)

Vol. 3, Issue 11, November 2014

$$\begin{cases} V_d = V \\ V_q = 0 \end{cases} \quad (24)$$

In practice, the grid voltage is nonsinusoidal due to harmonics. Therefore, both V_d and V_q will not be constant but have slight ripples whose frequencies and magnitudes depend on the harmonic components. However, in steady state, the average value of V_q is still equal to zero. Consequently, (23) can be rewritten as (25). Its active power depends on the d -axis current, and the reactive power depends on the q -axis current. Furthermore, in order to achieve unity power factor fundamental current flow, the q component of the command current vector is set to zero

$$\begin{cases} P = \frac{3}{2}(v_d i_d) \\ Q = \frac{3}{2}(v_d i_q) \end{cases} \quad (25)$$

Assuming lossless power transmission between solar array and grid line, the relationship of instantaneous active power exchanged between the PV array and the grid is given by

$$P_{pv} = P = \frac{3}{2}(v_d i_d) \quad (26)$$

This allows one to obtain the relation

$$i_d = \frac{2}{3v_d} P_{pv} \quad (27)$$

Therefore, the PV power information can be obtained from the d -axis grid current component by the relation (27).

B. Signal Error of Outer Voltage Regulator

The change of d -axis current in one period sampling T_e under irradiation variation is expressed by the following:

$$\Delta i_d(k) = \Delta i_v(k) + \Delta i_G(k) \quad (28)$$

$\Delta i_v(k)$ is the change of d -axis current component caused by the tracker perturbation, and $\Delta i_G(k)$ is the change of d -axis current component caused by the change in irradiation Fig. 7. Thus, the dc bus-voltage control loop under changing irradiation can be modeled with the block diagram of Fig. 8, where the current of PV array is an input disturbance. In this case, the error

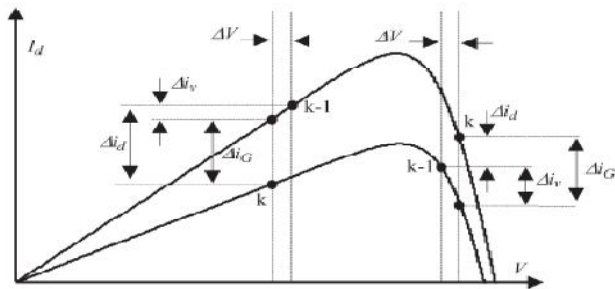


Fig. 7. I_d - V characteristic under variable irradiation

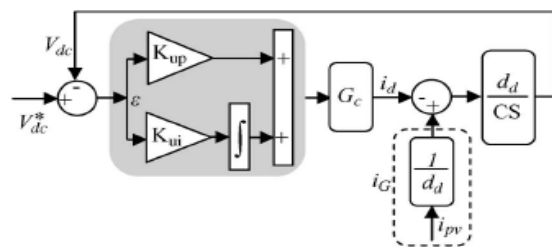


Fig. 8. Voltage loop diagram under variable irradiation.

between voltage reference V_{dc}^* and voltage measurement V_{dc} is the following:

$$\varepsilon(s) = A(s)V_{dc}^*(s) + B(s)i_G(s) \quad (29)$$

where

$$A(s) = \frac{cS^2}{cS^2 + d_d k_{up} S + d_d k_{ui}}$$

$$B(s) = \frac{d_d}{c} \frac{s}{s^2 + \frac{d_d k_{up}}{c} s + \frac{d_d k_{ui}}{c}}$$

If we consider only the impact of perturbation i_G , we can write

$$\varepsilon(s) = \frac{d_d}{c} \frac{s}{s^2 + \frac{d_d k_{up}}{c} s + \frac{d_d k_{ui}}{c}} i_G(s) \quad (30)$$

Assuming that the rate of change in the irradiation is constant over one sampling period T_e of the MPPT ($\Delta i_G = \alpha T_e$), the $i_G(s)$ expression can be written

$$i_G(s) = \frac{\alpha}{s^2} \tag{31}$$

By inserting (31) into (30), the error is defined as

$$\varepsilon(s) = \frac{d_d}{c} \frac{s}{s^3 + \frac{d_d k_{up}}{c} s^2 + \frac{d_d k_{ui}}{c} s} \tag{32}$$

To calculate the signal error, we use the final value theorem for Laplace transforms. According to this theorem, as long as $\varepsilon(s)$

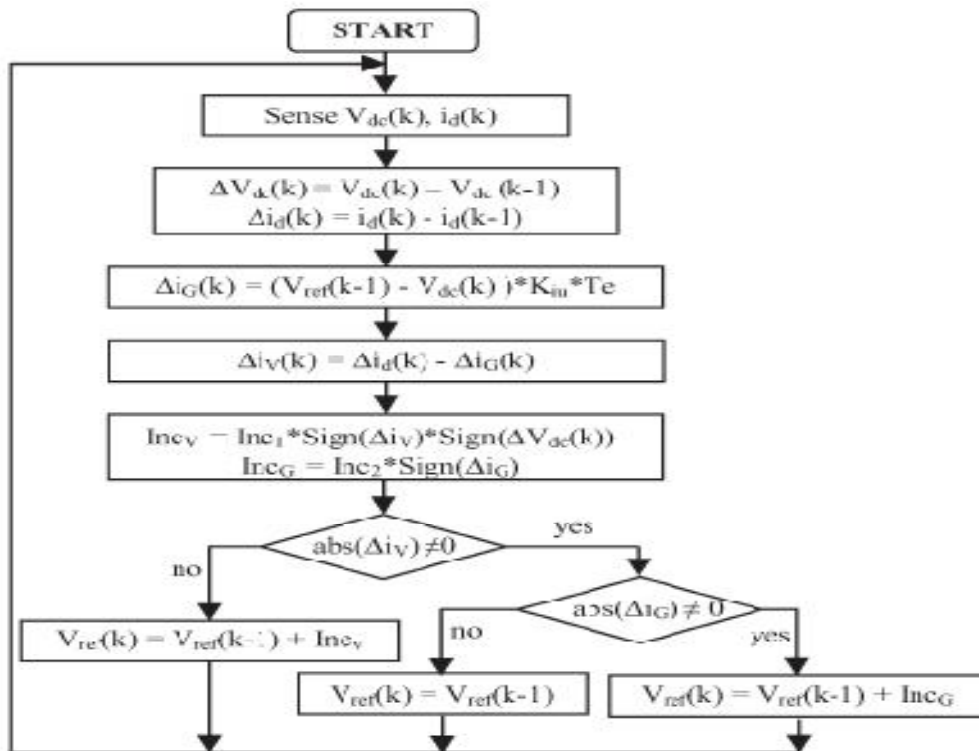


Fig. 9. Flowchart of the proposed MPPT algorithm.

does not have any poles in the right half of the complex plane, except maybe $s = 0$, then

$$\varepsilon = \lim_{s \rightarrow 0} \left[\frac{d_d}{c} \frac{s}{s^2 + \frac{d_d k_{up}}{c} s + \frac{d_d k_{ui}}{c}} \right] \tag{33}$$

Hence, the signal error has the following form (Fig. 9):

$$\varepsilon = \frac{\alpha}{k_{ui}} \tag{34}$$

Finally, the $\Delta i_G(k)$ that reflects only the change in power caused by the irradiation variation is defined as in

$$\Delta i_G = T_e \cdot \varepsilon \cdot k_{ui} = T_e \cdot k_{ui} \cdot (V_{dc}^*(k-1) - V_{dc}(k)) \tag{35}$$

The flowchart of the proposed MPPT is shown in Fig. 9. The first step is to set up a fixed voltage whose value is about 0.8 times of the PV array open-circuit voltage. Then, the instantaneous voltage of the PV array and the d -axis grid current component are measured using the saved previous voltage and current in order to calculate the differential values of Δi_d and ΔV_{dc} . After that, the Δi_G and Δi_V are calculated by using (35) and (28), respectively. With this information, two increments are calculated. The first Inc_V will be used when the PV array voltage is far away from the MPP voltage and the second Inc_G when irradiance change is present and the PV array voltage is initially equal to the voltage of the MPP. In the next test, if $abs(\Delta i_V)$ is more than zero (the power change caused by the previous tracker perturbation is different from zero), the reference voltage of the PV array is given by adding Inc_V to the previous reference voltage (Inc_V can be positive or

International Journal of Advanced Research in Electrical, Electronics and Instrumentation Engineering

(An ISO 3297: 2007 Certified Organization)

Vol. 3, Issue 11, November 2014

IV. MODELLING OF CASE STUDY AND SIMULATION RESULTS

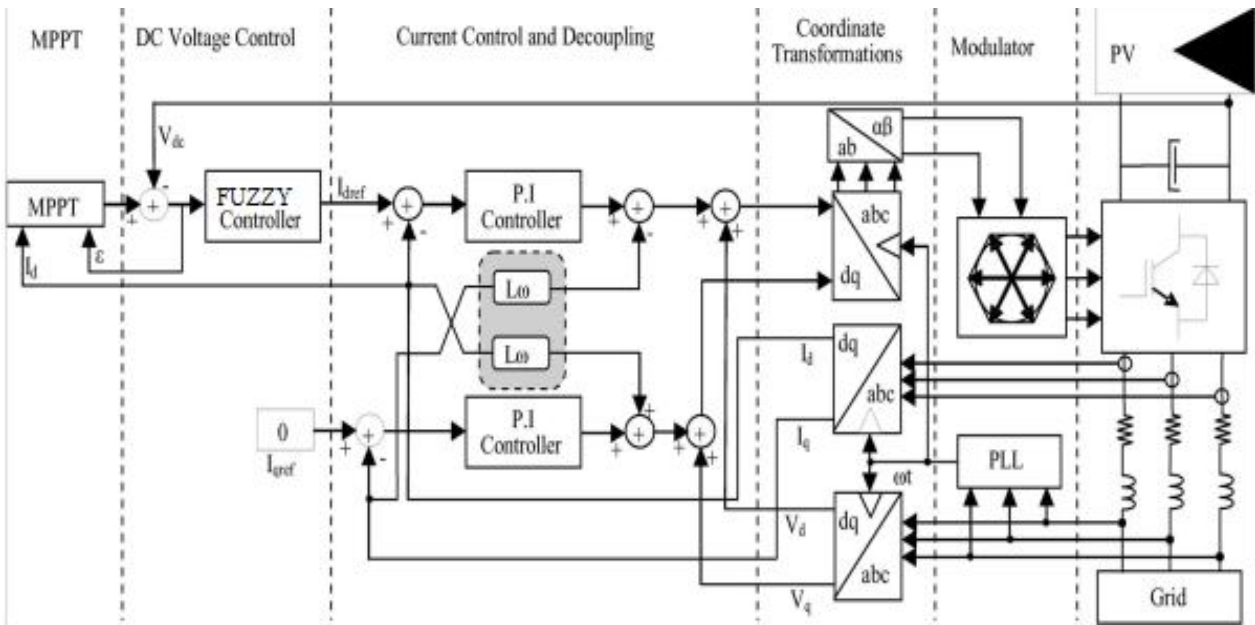


Fig. 10 Modal Grid-connected PV system with fuzzy controller

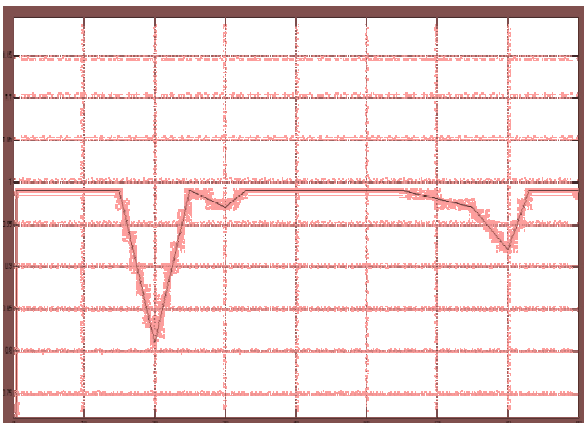


Fig. 11 Simulation Measurements of the instantaneous efficiency the instantaneous efficiency with modified MPPT using FUZZY Controller.

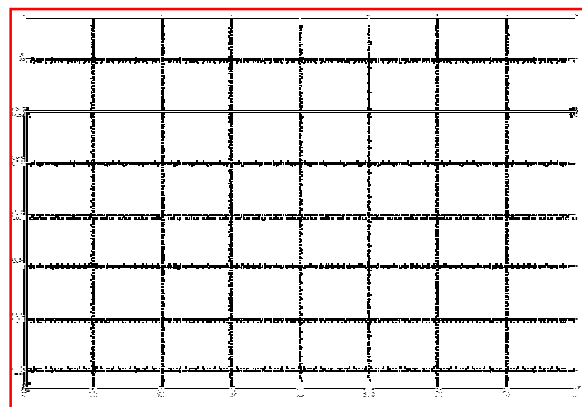


Fig. 12. Simulation measurement of using PI controller

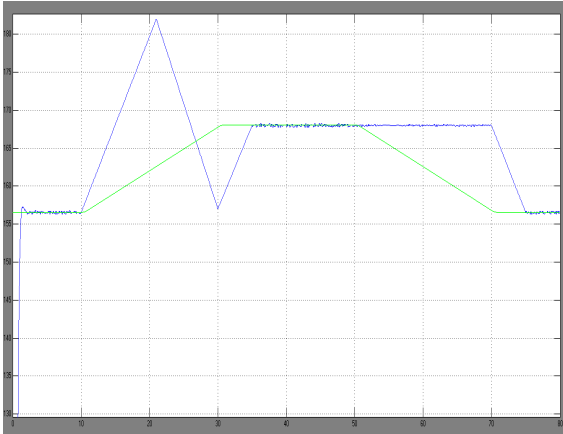


Fig.13 PV array voltage with classical P&O and theoretical MPP modified MPPT and theoretical

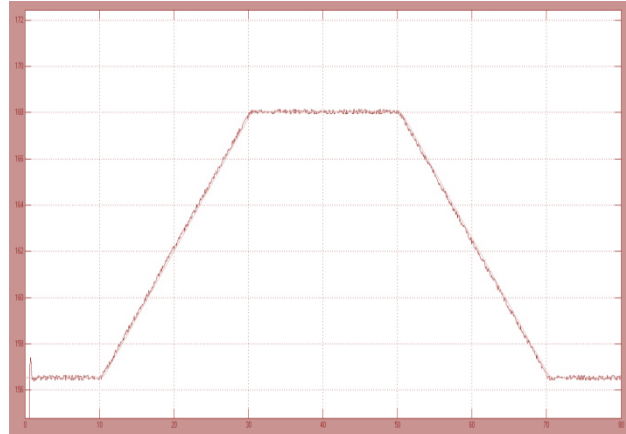


Fig. 14. PV system voltage with the voltage during a trapezoidal irradiation profile. MPP voltage during a trapezoidal irradiation

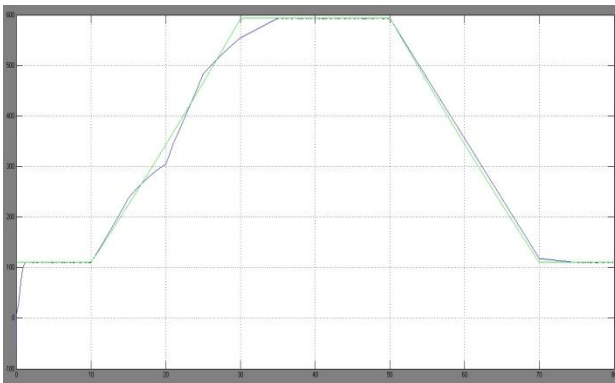


Fig. 15. Simulation measurement of the PV array power during a PV array power during trapezoidal irradiation profile, using the classical P&O MPPT the classical method, compared to the theoretical MPP power.

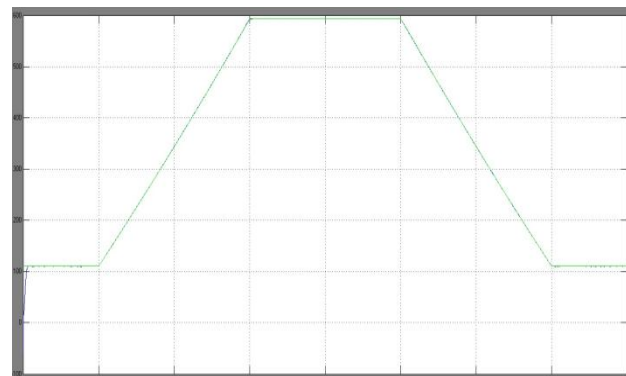


Fig. 16. Experimental measurement of the a trapezoidal irradiation profile, using P&O MPPT method, compared to the theoretical MPP power.

From the above simulated results we can identify the instantaneous efficiency with modified MPPT using FUZZY Controller , PV system voltage with the modified MPPT and theoretical MPP voltage during a trapezoidal irradiation profile and PV array power during a trapezoidal irradiation profile using the classical P&O MPPT method, compared to the theoretical MPP power are improved.

Fuzzy logic control circuit is implemented in MAT LAB is shown in below fig.

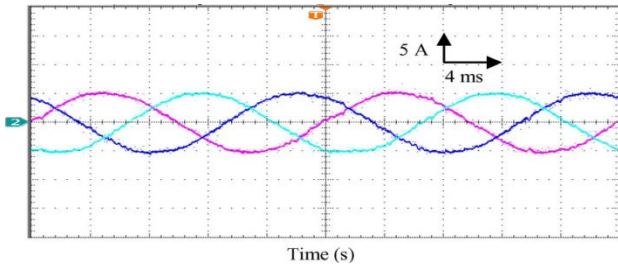


Fig. 17. Steady-state inverter output current.

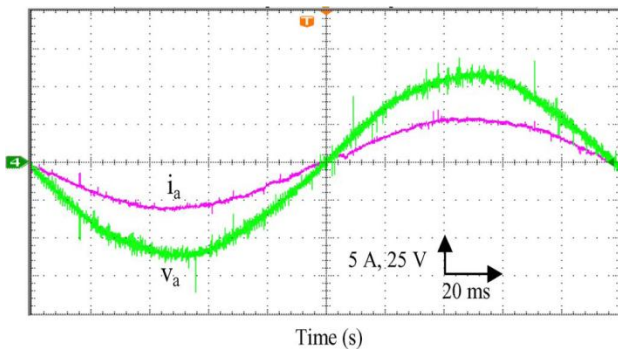


Fig. 18. Grid voltage and grid current at unity power factor.

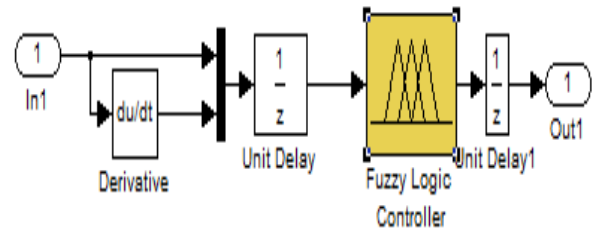


Fig. 19 Fuzzy Logic Circuit

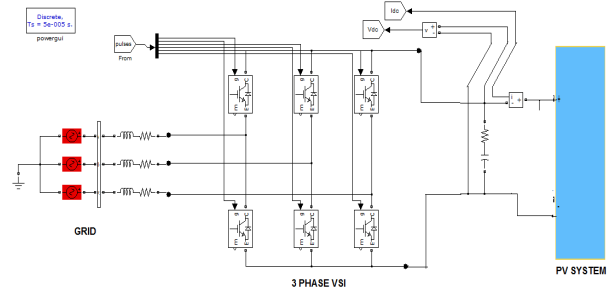


Fig. 20 Grid connected PV system through VSI
MAT Lab based simulation circuit

This section presents the simulation results of the classical P&O and the proposed method in order to validate the performance of the control scheme. Computer simulation has been done using *MATLAB/SIMULINK* simulation package. The full diagram of the control methodology and the modulation is shown in Fig. 10. The characteristics of Solar PV module are used for the PV array model in the simulation and experiment. The 60 module provides 60 W of nominal maximum power and a 21.1-V open-circuit voltage at an irradiation of 1 kW/m² and an ambient temperature of 25 °C. To compare the performance of the proposed MPPT method with that of the P&O method, the simulations are configured under exactly the same conditions to compare the performances. The PV array in simulation is composed of ten series connected modules. The sampling period used for MPPT algorithm is chosen as 0.2 s, and voltage increments of $Inc1 = 0.5$ V and $Inc2 = 0.1$ V are used. In order to verify the effect of rapidly changing irradiation, an irradiation ramp change was used. A 20-s period for the increasing and decreasing ramps was selected. This irradiation change starts from 200 W/m², stops at 1000 W/m², waits at this level for 20 s, and decreases again back to 200 W/m² with a constant slope. The temperature is considered constant during the simulation.

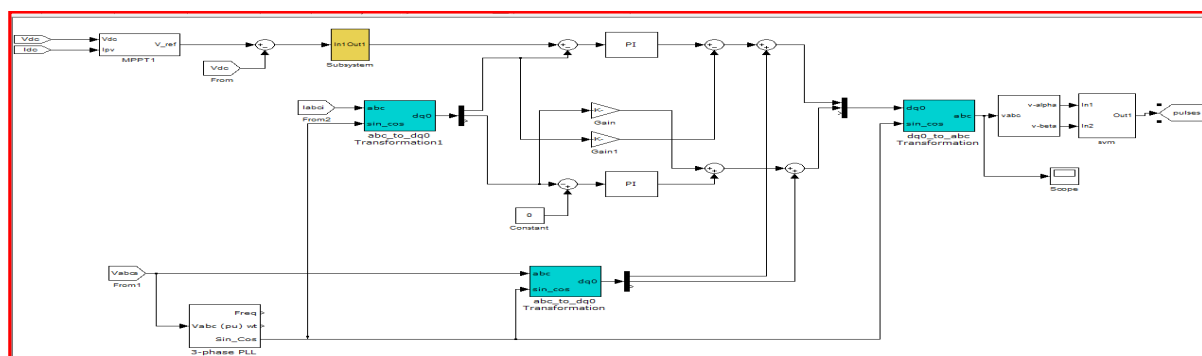


Fig. 21SRF Configuration circuit



International Journal of Advanced Research in Electrical, Electronics and Instrumentation Engineering

(An ISO 3297: 2007 Certified Organization)

Vol. 3, Issue 11, November 2014

V. CONCLUSION

In order to avoid possible mistakes of the classical MPPT algorithm with PI control due to the fast-changing irradiation, this paper a FUZZY based MPPT-SRF Configuration of a Single Stag Grid-Connected PV System Inverter Based On Voltage-Oriented Control has proposed an improved MPPT controller. Our control scheme uses the d -axis grid current component and the signal error of the FUZZY outer voltage regulator. This MPPT method permits one to differentiate the contribution of increment perturbation and irradiation change in power variation, hence identifying the correct direction of the MPP. In the simulation and experimental results, the robust tracking capability under rapidly increasing and decreasing irradiance has been proved. Moreover, the output power losses caused by the dynamic tracking errors are drastically reduced, particularly under fast changing irradiation. With proposed fuzzy controller we achieved improved wave shapes in ac voltages and also maintain unity power factor.

REFERENCES

- [1] Riad Kadri, Jean-Paul Gaubert, *Member, IEEE*, and Gerard Champenois, *Member, IEEE* "An Improved Maximum Power Point Tracking for Photovoltaic Grid-Connected Inverter Based on Voltage-Oriented Control" IEEE TRANSACTIONS ON INDUSTRIAL ELECTRONICS, VOL. 58, NO. 1, JANUARY 2011
- [2] C. Meza, J. J. Negroni, D. Biel, and F. Guinjoan, "Energy-balance modeling and discrete control for single-phase grid-connected PV central inverters," *IEEE Trans. Ind. Electron.*, vol. 55, no. 7, pp. 2734–2743, Jul. 2008.
- [3] B. Sahan, A. N. Vergara, N. Henze, A. Engler, and P. Zacharias, "A singlestage PV module integrated converter based on a low-power currentsource inverter," *IEEE Trans. Ind. Electron.*, vol. 55, no. 7, pp. 2602–2609, Jul. 2008.
- [4] K. Hemmes, "Towards multi-source multi-product and other integrated energy systems," *Int. J. Integr. Energy Syst.*, vol. 1, no. 1, pp. 1–15, Jan.–Jun. 2009.
- [5] F. Liu, Y. Zhou, S. Duan, J. Yin, B. Liu, and F. Liu, "Parameter design of a two-current-loop controller used in a grid-connected inverter system with LCL filter," *IEEE Trans. Ind. Electron.*, vol. 56, no. 11, pp. 4483–4491, Nov. 2009.
- [6] T. Shimizu, O. Hashimoto, and G. Kimura, "A novel high-performance utility-interactive photovoltaic inverter system," *IEEE Trans. Power Electron.*, vol. 18, no. 2, pp. 704–711, Mar. 2003.
- [7] T. Esumi, J. W. Kimball, P. T. Krein, P. L. Chapman, and P. Midya, "Dynamic maximum power point tracking of photovoltaic arrays using ripple correlation control," *IEEE Trans. Power Electron.*, vol. 21, no. 5, pp. 1282–1291, Sep. 2006.
- [8] N. Femia, G. Petrone, G. Spagnuolo, and M. Vitelli, "Optimization of perturb and observe maximum power point tracking method," *IEEE Trans. Power Electron.*, vol. 20, no. 4, pp. 963–973, Jul. 2005.
- [9] G. Carannante, C. Fraddanno, M. Pagano, and L. Piegari, "Experimental performance of MPPT algorithm for photovoltaic sources subject to inhomogeneous insolation," *IEEE Trans. Ind. Electron.*, vol. 56, no. 11, pp. 4374–4380, Nov. 2009.
- [10] N. Femia, G. Petrone, G. Spagnuolo, and M. Vitelli, "Perturb and observe MPPT technique robustness improved," in *Proc. IEEE Int. Symp. Ind. Electron.*, 2004, vol. 2, pp. 845–850.
- [11] K. H. Hussein, I. Muta, T. Hoshino, and M. Osakada, "Maximum photovoltaic power tracking: An algorithm for rapidly changing atmospheric conditions," *Proc. Inst. Elect. Eng.—Gener., Transm. Distrib.*, vol. 142, no. 1, pp. 59–64, Jan. 1995.
- [12] N. Femia, G. Petrone, G. Spagnuolo, and M. Vitelli, "A technique for improving P&O MPPT performances of double-stage grid-connected photovoltaic systems," *IEEE Trans. Ind. Electron.*, vol. 56, no. 11, pp. 4473–4482, Nov. 2009.

BIOGRAPHY



I.D.V.Koteswara Rao currently pursuing his M.Tech., in Power Electronics And Drives from JNT University, Kakinada. He had done his B.Tech degree from B.V.S.R Engineering college, Affiliated to JNT University, Kakinada in 2012 and his fields of interest include, Power Electronics.



2.O.RANJIT KUMAR has completed his B.Tech in Electrical & Electronics Engineering in 2009, M.TECH in Power & Industrial Drives, and presently he is pursuing his PH.D. He is working as Assistant Professor in EEE department at QIS Institute of Technology, Ongole, A.P, India. His area of interest include, power electronics & Electrical Drives.